High-contrast terahertz modulator based on extraordinary transmission through a ring aperture

Jie Shu, Ciyuan Qiu, Victoria Astley, Daniel Nickel, Daniel M. Mittleman, and Qianfan Xu*

Department of Electrical and Computer Engineering, Rice University, Houston, Texas 77005, USA
[*]qianfan@rice.edu

Abstract: We demonstrated extraordinary THz transmission through ring apertures on a metal film. Transmission of 60% was obtained with an aperture-to-area ratio of only 1.4%. We show that the high transmission can be suppressed by over 18 dB with a thin layer of free carriers in the silicon substrate underneath the metal film. This result suggests that CMOS-compatible terahertz modulators can be built by controlling the carrier density near the aperture.

OCIS codes: (120.7000) Transmission; (260.5740) Resonance; (300.6495) Spectroscopy, terahertz; (200.6715) Switching.

References and links

1. W. L. Chan, K. Charan, D. Takhar, K. F. Kelly, R. G. Baraniuk, and D. M. Mittleman, "A single-pixel terahertz imaging system based on compressed sensing," Appl. Phys. Lett. **93**(12), 121105 (2008).
2. T. Kleine-Ostmann, K. Pierz, G. Hein, P. Dawson, and M. Koch, "Audio signal transmission over THz communication channel using semiconductor modulator," Electron. Lett. **40**(2), 124 (2004).
3. C. Jastrow, K. Munter, R. Piesiewicz, T. Kurner, M. Koch, and T. Kleine-Ostmann, "300 GHz transmission system," Electron. Lett. **44**(3), 213 (2008).
4. R. Kersting, G. Strasser, and K. Unterrainer, "Terahertz phase modulator," Electron. Lett. **36**(13), 1156 (2000).
5. I. H. Libon, S. Baumgartner, M. Hempel, N. E. Hecker, J. Feldmann, M. Koch, and P. Dawson, "An optically controllable terahertz filter," Appl. Phys. Lett. **76**(20), 2821 (2000).
6. H.-T. Chen, W. J. Padilla, J. M. O. Zide, A. C. Gossard, A. J. Taylor, and R. D. Averitt, "Active terahertz metamaterial devices," Nature **444**(7119), 597–600 (2006).
7. W. L. Chan, H.-T. Chen, A. J. Taylor, I. Brener, M. J. Cich, and D. M. Mittleman, "A spatial light modulator for terahertz beams," Appl. Phys. Lett. **94**(21), 213511 (2009).
8. M. Seo, J. Kyoung, H. Park, S. Koo, H. S. Kim, H. Bernien, B. J. Kim, J. H. Choe, Y. H. Ahn, H. T. Kim, N. Park, Q. H. Park, K. Ahn, and D. S. Kim, "Active terahertz nanoantennas based on VO2 phase transition," Nano Lett. **10**(6), 2064–2068 (2010).
9. H.-T. Chen, H. Lu, A. K. Azad, R. D. Averitt, A. C. Gossard, S. A. Trugman, J. F. O'Hara, and A. J. Taylor, "Electronic control of extraordinary terahertz transmission through subwavelength metal hole arrays," Opt. Express **16**(11), 7641–7648 (2008).
10. E. Hendry, M. J. Lockyear, J. Gómez Rivas, L. Kuipers, and M. Bonn, "Ultrafast optical switching of the THz transmission through metallic subwavelength hole arrays," Phys. Rev. B **75**(23), 235305 (2007).
11. Y. Poujet, J. Salvi, and F. I. Baida, "90% Extraordinary optical transmission in the visible range through annular aperture metallic arrays," Opt. Lett. **32**(20), 2942–2944 (2007).
12. Y.-T. Chang, D.-C. Tzuang, Y.-T. Wu, C.-F. Chan, Y.-H. Ye, T.-H. Hung, Y.-F. Chen, and S.-C. Lee, "Surface plasmon on aluminum concentric rings arranged in a long-range periodic structure," Appl. Phys. Lett. **92**(25), 253111 (2008).
13. Q. Xu, B. Schmidt, S. Pradhan, and M. Lipson, "Micrometre-scale silicon electro-optic modulator," Nature **435**(7040), 325–327 (2005).
14. Q. Xu, S. Manipatruni, B. Schmidt, J. Shakya, and M. Lipson, "12.5 Gbit/s carrier- injection-based silicon micro-ring modulators," Opt. Express **15**(2), 430–436 (2007).
15. F. J. Garcia-Vidal, L. Martin-Moreno, T. W. Ebbesen, and L. Kuipers, "Light passing through subwavelength apertures," Rev. Mod. Phys. **82**(1), 729–787 (2010).
16. F. J. García-Vidal, E. Moreno, J. A. Porto, and L. Martín-Moreno, "Transmission of light through a single rectangular hole," Phys. Rev. Lett. **95**(10), 103901 (2005).
17. X. A. Xiao, W. Jinbo, Y. Sasagawa, F. Miyamaru, M. Y. Zhang, M. W. Takeda, C. Y. Qiu, W. J. Wen, and P. Sheng, "Resonant terahertz transmissions through metal hole array on silicon substrate," Opt. Express **18**(18), 18558–18564 (2010).

18. H. Cao and A. Nahata, "Influence of aperture shape on the transmission properties of a periodic array of subwavelength apertures," Opt. Express **12**(16), 3664–3672 (2004).
19. D. Qu, D. Grischkowsky, and W. Zhang, "Terahertz transmission properties of thin, subwavelength metallic hole arrays," Opt. Lett. **29**(8), 896–898 (2004).
20. M. A. Seo, H. R. Park, S. M. Koo, D. J. Park, J. H. Kang, O. K. Suwal, S. S. Choi, P. C. M. Planken, G. S. Park, N. K. Park, Q. H. Park, and D. S. Kim, "Terahertz field enhancement by a metallic nano slit operating beyond the skin-depth limit," Nat. Photonics **3**(3), 152–156 (2009).
21. Y. M. Bahk, H. R. Park, K. J. Ahn, H. S. Kim, Y. H. Ahn, D. S. Kim, J. Bravo-Abad, L. Martin-Moreno, and F. J. Garcia-Vidal, "Anomalous band formation in arrays of terahertz nanoresonators," Phys. Rev. Lett. **106**(1), 013902 (2011).
22. D. Mittleman, *Sensing with Terahertz Radiation,* (Springer-Verlag, 2002).
23. J. O. Smith, *Mathematics of the Discrete Fourier Transform (DFT) with Audio Applications*, (W3K Publishing, 2007).

1. Introduction

Modulators for quasi-optical terahertz (THz) beams have various applications in imaging and communications [1–3]. Different types of THz modulators have been demonstrated including those based on quantum-well structures [4, 5] and those based on metallic antenna structures on semiconductor substrates [6–10]. Among them, the modulators based on the extraordinary optical transmission (EOT) effect [8–10] of sub-wavelength apertures in a metal film are of particular interest, because they can show high extinction ratio up to 40 dB [8]. The switching effects were achieved either with dielectric–metal phase transition of VO_2 [8], or by changing the free-carriers density in a semiconductor substrate underneath the film [9, 10].

In these previous demonstrations, the modulators have a metal layer that is fully connected [8–10]. Therefore, to build an electro-optic switch, the metal layer can only be used as one electrode [9]. With the other electrode placed far away, the speed and power efficiency of the switch is limited. Here we demonstrate a ring aperture design where the metal inside and outside of the ring are electrically isolated and can be used as two electrodes [11, 12]. This capability will allow us to electrically control the carrier density only in the area underneath the aperture. Comparing to controlling the carrier density in the whole area underneath the metal, this design minimizes the power consumption and maximizes the operation speed.

We show experimentally that transmission of 60% can be obtained for an aperture array with only 1.4% open area. The high transmission can be suppressed by over 18 dB with a thin layer of free carriers in the silicon substrate underneath the metal film. Simulations show that the isolated metal film in the center of the aperture can be connected electrically with a metal wire bridged across the aperture on top (Fig. 1(a)) without significantly affecting the transmission characteristics. A p-i-n junction similar to that used in near-infrared optical switches [13] can be used to control the carrier density just beneath the aperture (Fig. 1(b)). The p-i-n junction can introduce larger change in the number of carriers in the aperture region than the carrier depletion junctions used in [9]. We expect that a switching speed on the order of 10 Gbps can be achieved with this type of junction [14]. This design is also compatible with pixelation, providing the opportunity for building a high speed high contrast terahertz spatial light modulator [7]. With these capabilities, the electrical control of free-space terahertz beams begins to approach the level of control achieved by conventional modulators in the visible and near-infrared.

2. Principle of operation

EOT is an optical phenomenon in which a structure containing subwavelength apertures in a metal film transmits more light than that expected on the basis of ray optics. EOT through narrow apertures is due to a significantly enhanced electric field inside and around the aperture. Because of the strong local field, the EOT effect is highly sensitive to the change in material properties around the aperture, which is desirable for such applications as molecular sensing, spectroscopy and optical switching [15, 16]. The EOT phenomenon is especially strong in the THz frequency range since apertures with width orders-of-magnitude smaller than the wavelength can be made [17–21].

To understand the principle of operation, the E-field amplitude of the TE_{11} mode of a ring aperture with a radius $r = 50$ µm and a width of $w = 1$ µm is shown in Fig. 1(c). The phase of the E_r component of the mode varies by 2π over the circumference of the ring. This mode thus has a cut-off frequency $f_c = c/(2\pi r \cdot n_{eff})$, where n_{eff} is the effective index. At that frequency, there is no phase variation in the direction perpendicular to the substrate, creating a Fabry-Perot (FP) resonance as waves travelling back and forth inside the aperture, which results in the resonating EOT effect. The yellow arrows in the figure show the direction of E-field of the y-polarized TE_{11} mode. One can see that the E-field at upper and lower halves of the ring both point to the $+y$ direction; therefore, this mode will efficiently couple to a y-polarized normal-incidence plane wave. The degenerate x-polarized TE_{11} mode of the aperture provides EOT for the x-polarized normal-incident wave, resulting in polarization-independent operation.
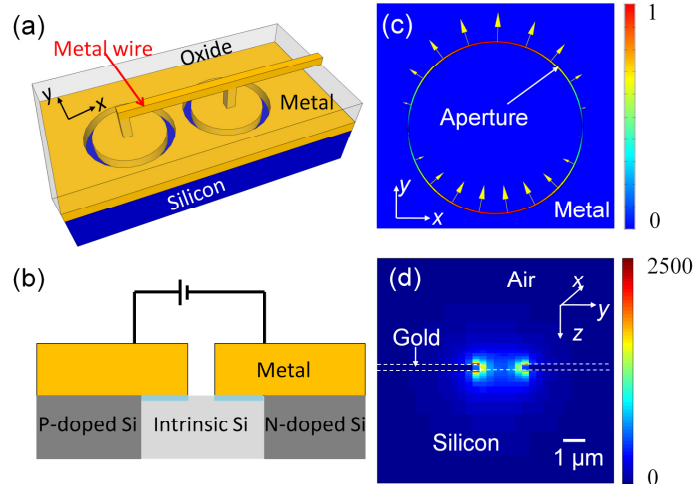

Fig. 1. (a) Schematic design of the proposed modulator. The central metal pads inside the apertures are connected by metal wire bridges to form one electrode. The continuous metal film outside of the apertures is used as another electrode. (b) Cross-sectional view of the ring aperture with a p-i-n junction embedded in the silicon substrate underneath. (c) Top-view of the E-field distribution of the TE_{11} mode in the ring. (d) side-view of the E-field intensity distribution when a plane waves passes through the ring aperture.

The ring aperture also supports a TEM mode. However, the TEM mode does not have a cut-off frequency to support EOT, and cannot be excited by a normal-incidence plane wave because its E-field at opposite sides of the ring points to opposite directions.

3. FDTD simulation

We performed a 3D finite-difference-time-domain (FDTD) simulation of a normally-incident broadband THz wave passing through the aperture in a gold film on an intrinsic silicon substrate. In the simulation, periodic boundary conditions were used assuming a square-lattice array with lattice constant $p = 150$ µm. The simulation shows strong E-field enhancement around the aperture. Figure 1(d) shows the side view of the resonant E-field intensity distribution when a plane wave passes through the ring aperture. The E-field distribution is highly confined in and around the aperture, with the peak E-field average intensity ($|E|^2$) in the aperture enhanced by ~2500 times comparing to the incident wave.

The simulated power transmission spectra for different apertures are shown in Fig. 2(a). As the theory predicts, the cavity resonant frequency scales inversely with the circumference of the rings. The peak transmission varies between 62% and 71% even though the apertures only comprises 1.1%-1.9% of the area. The peak transmission is limited by the large difference in refractive index between air on top of the film and silicon beneath the metal film. The peak transmission would be close to 100% if the refractive indices on both sides of the metal film were the same. When the width of the aperture varying between 20 µm and 1

μm, or when the thickness of metal varying between 2 μm and 100 nm, only small changes (<6%) in the peak transmission of the aperture are observed. These small variations are mainly due to changes in optical loss in the metal. Simulations also confirm that the resonant wavelength is not sensitive to the shape of the aperture. To show that, we computed the simulated transmission spectrum of square rings (dashed lines in Fig. 2(a)). Comparing to the circular rings with the same circumference, the resonant frequency and peak transmission of the square rings only change slightly. We also note that the spectra of all the apertures show smaller and narrower peaks around 0.57 THz. The frequency of these features only changes with the periodicity of the pattern, showing that they are from the grating effect.
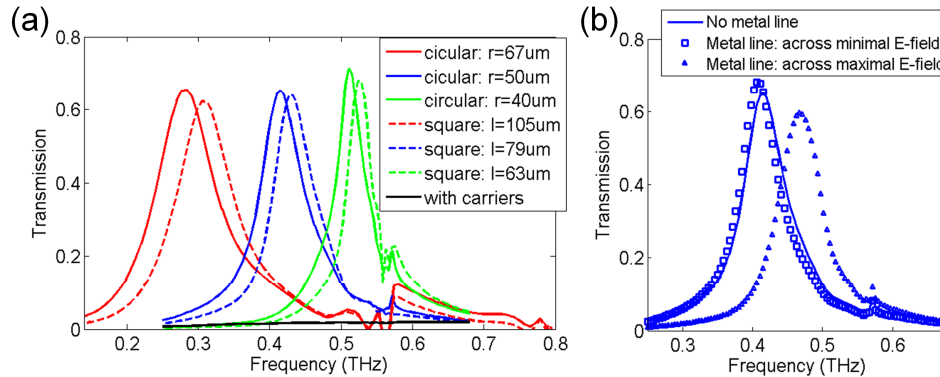

Fig. 2. (a) Simulated power transmission spectra of 2D arrays of circular and square ring apertures in a gold film on an intrinsic silicon wafer. Apertures width $w = 1$ μm and the period is $p = 150$ μ m. r: radius of a circular aperture, l: the side length of a square aperture. The black solid line close to the bottom shows the transmission when the silicon underneath the aperture has carrier density of 3×10^{17} cm^{-3}. (b) Simulated transmission spectra of a ring aperture array with a 1-μm-wide gold line placed 1-μm above the metal film.

To switch off the EOT effect, one can inject free carriers into silicon underneath the apertures [9, 10, 13]. A small increase in free-carrier absorption is significantly enhanced by the FP resonance, resulting in a substantial decrease in transmission. The black solid line in Fig. 2(a) shows the simulated transmission spectrum when free carriers with a density of 3×10^{17} cm^{-3} are injected into a 1-μm-deep and 4-μm-wide region of silicon under the ring aperture, giving rise to a local conductivity of ~10 $\Omega^{-1}\cdot$cm^{-1}. These carriers cause the transmission of the aperture to drop as much as 17 dB, while the one-pass absorption of the free carriers is only ~0.6 dB. Because the E-field is highly confined around the aperture, the p- and n- doped areas shown in Fig. 1(b) do not cause significant loss as long as they are placed a few microns away from the aperture.

To use the metal inside the aperture as an electrode, it needs to be electrically connected to a vertical via and a metal wire going across the aperture on top of a dielectric material. To see how this metal line would affect the transmission of the device, we added a 1-μm-wide gold line on top of a 1-μm-thick SiO$_2$ layer on the metal film, as shown in Fig. 1(a). If the wire crosses the aperture at the position with the minimal E-field, the transmission is barely affected as shown by the blue squares in Fig. 2(b). If the wire crosses the aperture at the position with the maximal E-field, simulations (triangles in Fig. 2(b)) show a ~10% blue shift of the resonant peak and a ~10% drop of the peak transmission.

4. Device fabrication

We fabricated periodic arrays of circular and square ring arrays with various width w and radius r (or side length l for square rings) by E-beam lithography. The period of all the arrays is $p = 150$ μm. The pattern is first defined on the E-beam resist SU-8 on a 500-μm-thick high-resistivity silicon substrate. A 100-nm-thick gold film is then evaporated on the patterned resist, followed by a lift-off process. The SEM pictures of the fabricated circular and square

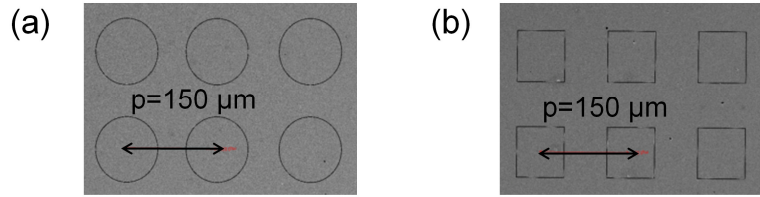ring arrays are shown in Fig. 3(a) and Fig. 3(b), respectively. The total size of each array is 4.8 mm × 4.8 mm.

(a)

(b)

p=150 μm

p=150 μm

Fig. 3. (a) An SEM picture of fabricated circular ring array with w = 1μm, p = 150 μm, r = 50 μm. (b) An SEM picture of fabricated square ring array with w = 1μm, p = 150 μm, l = 79 μm.

5. Measurements

The transmission of the device, measured using a time domain THz spectrometer [22], agrees well with the simulation results. Figure 4(a) compares the time-domain transmitted field amplitude signals of an aperture array (red) with that of a bare silicon substrate (blue). The time domain signals were truncated at 10 ps after the peak of the initial pulse to remove the signal reflected from the back of the substrate. Then, a Fourier transform with zero-padding [23] is performed to obtain the transmission spectra. Figure 4(b) compares the measured (solid) and simulated (dashed) power transmission spectra. The blue solid line in Fig. 4(b) shows the measured power transmission spectrum of rings with r = 50 µm, normalized to the transmission of a bare high-resistivity silicon substrate. A transmission peak centered at 0.42 THz can be clearly identified. The measured F-P cavity resonance peak is slightly broader than the simulated one, which may be due to size variation of rings in the array. The narrower surface resonance peak at 0.57 THz cannot be resolved in the measured spectra due to the limited time window length.
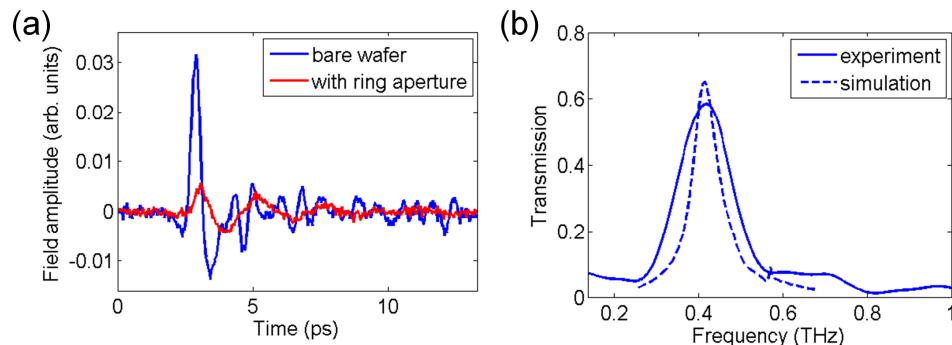

Fig. 4. (a) Measured time domain transmitted field amplitude signals of circular ring apertures with r = 50 µm on a high-resistivity silicon substrate (red) and that of a bare high-resistivity silicon substrate (blue). (b) Measured (solid) and simulated (dashed) power transmission spectra of the ring apertures, which is normalized to that of the bare silicon substrate.

Figure 5(a) compares the measured transmission spectra for different aperture patterns. Rings with different circumferences are shown in different colors. Their resonant frequencies scale inversely proportional to their circumference, as expected. Although the transmission decreases as the radius of ring aperture decreases, the normalized-to-area transmission increases due to larger field enhancement inside the ring cavity. We also verify that square-rings (dashed) have the similar resonant frequencies as the circular-rings (solid) with the same circumferences. Moreover, we measured the polarization dependency of the devices, as shown in Fig. 5(b) for circular ring aperture and Fig. 5(c) for square ring aperture. The measured power transmission spectra of ring arrays for different polarization angles of

incident THz beam show the same resonant frequency with transmission varying within 10%, verifying polarization independency of the devices due to the symmetry of the ring apertures.
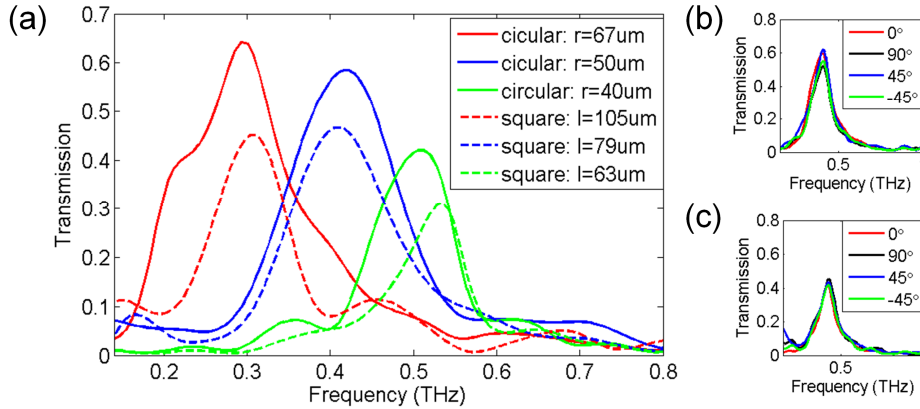

Fig. 5. (a) Measured power transmission spectra of 2D circular and squre ring aperture arrays. All the apertures have width of $w = 1$ µm and the period of all the arrays is $p = 150$um. r is the radius of a circular aperture, and l the side length of a square aperture. (b), (c) Polarization dependency: measured power transmission spectra of circular (b) and square (c) ring aperture arrays for different polarization angles.

Using an ion-implanted substrate, we show that EOT can be efficiently suppressed with a thin layer of free carriers underneath the apertures. We fabricated the ring apertures on a silicon substrate implanted with boron ions. The designed hole density in silicon resulted from the implantation is shown in Fig. 6(a), which decreases from $\sim 10^{19}$ cm^{-3} at the surface to almost 0 in a depth of less than 200 nm. With the implantation, the EOT transmission of the ring apertures drops over 18 dB. The measured transmission spectra on the implanted, shown as the dashed lines in Fig. 6(b), are close to the noise level of the measurement system. In comparison, the one-pass absorption of the free carriers is measured to be only ~ 1.2 dB.
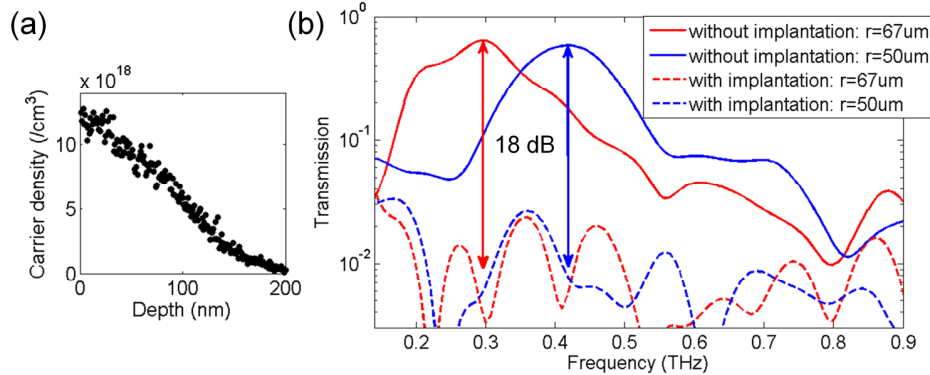

Fig. 6. (a) Carrier density distribution in silicon substrate with ion implantation of Boron atoms. (b) Measured power transmission spectra of different aperture with $w = 1$ µm and $p = 150$um on high-resistivity wafer (solid) and on high-conductivity wafer (dashed).

6. Conclusions

In conclusion, we demonstrate the EOT effect of ring apertures on a metal film for switching THz waves. We show that the transmission can be efficiently suppressed with a thin layer of free carriers in the silicon substrate underneath the metal film. These results suggest the possibility of CMOS-compatible THz-wave modulators with high speed and high on-off contrast ratios.